Theoretical Study of Binding Interactions and Vibrational Raman Spectra of Water in Hydrogen-Bonded Anionic Complexes: $(H_2O)_n^-$ (n = 2 and 3), $H_2O\cdots X^-$(X = F, Cl, Br, and I), and $H_2O\cdots M^-$ (M = Cu, Ag, and Au)

De-Yin Wu,*,† Sai Duan,† Xiu-Min Liu,† Yong-Chun Xu,† Yu-Xiong Jiang,† Bin Ren,‡ Xin Xu,‡ S. H. Lin,§ and Zhong-Qun Tian‡

Department of Chemistry, College of Chemistry and Chemical Engineering and State Key Laboratory of Physical Chemistry for Solid Surface, Xiamen University, Xiamen 361005, Fujian, People Republic of China, and Institute of Atomic and Molecular Sciences, Academia Sinica, Taipei 106, Taiwan, Republic of China

Received: March 20, 2007; In Final Form: October 9, 2007

Binding interactions and Raman spectra of water in hydrogen-bonded anionic complexes have been studied by using the hybrid density functional theory method (B3LYP) and ab initio (MP2) method. In order to explore the influence of hydrogen bond interactions and the anionic effect on the Raman intensities of water, model complexes, such as the negatively charged water clusters ($(H_2O)_n^-$, n = 2 and 3), the water···halide anions ($H_2O\cdots X^-$, X = F, Cl, Br, and I), and the water−metal atom anionic complexes ($H_2O\cdots M^-$, M = Cu, Ag, and Au), have been employed in the present calculations. These model complexes contained different types of hydrogen bonds, such as O−H···X^-, O−H···M^-, O−H···O, and O−H···e^-. In particular, the last one is a dipole-bound electron involved in the anionic water clusters. Our results showed that there exists a large enhancement in the off-resonance Raman intensities of both the H−O−H bending mode and the hydrogen-bonded O−H stretching mode, and the enhancement factor is more significant for the former than for the latter. The reasons for these spectral properties can be attributed to the strong polarization effect of the proton acceptors (X^-, M^-, O, and e^-) in these hydrogen-bonded complexes. We proposed that the strong Raman signal of the H−O−H bending mode may be used as a fingerprint to address the local microstructures of water molecules in the chemical and biological systems.

Introduction

Vibrational Raman spectroscopy has been widely used to characterize and analyze the interactions of water with a solute molecule in chemistry and biochemistry.[1,2] In the gas phase or liquid phase of pure water, the Raman signals of the O−H stretching modes are much stronger than that of the bending mode.[3−5] However, the relative intensities can be changed significantly in the aqueous solutions containing halides[6−12] or hydrated electrons[13−20] and on the electrochemical interfaces.[21−27] Experimentally, an intense peak of the bending mode of water was observed in the halide solutions at the beginning of 1960s,[6−10] which was explained by the formation of the hydrogen bond (O−H···X^-) between the anions of the dissolved halides (X^-) and the solvent water.[7,10] To understand the (O−H···X^-) hydrogen bonding, different water-halide anion clusters have been studied by using the infrared spectroscopy and the UV−visible absorption spectroscopy.[28−30] These studies showed that charge transfers from the halide anions to the solvent water molecules took place, resulting in a red shift of the vibrational frequencies and an enhancement of the infrared intensities.[30−33] However, these studies were generally limited to the infrared spectra for the hydrogen-bonded O−H stretching mode. As a special anion, hydrated electrons significantly enhanced the Raman intensities of the librations and the intramolcular modes.[14−20] As compared to the bulk water, the enhancement factors were $\sim 2 \times 10^3$ folds for the O−H stretching modes and $\sim 3 \times 10^5$ folds for the H−O−H bending mode with a resonance excitation at 683 nm.[18]

Similarly, the surface-enhanced Raman spectra (SERS) exhibit a significant enhancement in the bending mode for water molecules adsorbed at the negatively charged coinage metal electrodes.[21−27] In these studies, the applied potentials were very negative to the potential of zero charge (PZC) of the corresponding electrodes.[22−26] At such negative potentials, water molecules were found to prefer an adsorption configuration with the H-end down to form a hydrogen bond of O−H···M^-,[25] rather than the adsorption configuration with the O-end down which happened in the potential region positive to the PZC. Although the adsorption configurations were suggested for the interfacial waters in some previous studies,[25,34] correlation of the changes of the Raman intensities with bondings of the interfacial water molecules relative to the bulk water molecules has never been made. The enhancement in the Raman intensities of the interfacial water molecules was interpreted by a photon-induced charge-transfer process so far.[27]

There are many theoretical studies reporting the infrared spectra of water cluster anions,[30,35−37] water−metal atoms or their anions,[38−44] and water−halide anions,[29,31,33,37,45] there are, however, only a few studies being reported on the changes of the Raman intensities of the intramolecular vibrational modes of water due to the hydrogen bonding interactions.[46−51] Knochenmuss and Leutwyler[47] predicted the Raman intensities of some

* To whom correspondence should be addressed. E-mail: dywu@xmu.edu.cn.

† Department of Chemistry, College of Chemistry and Chemical Engineering.

‡ State Key Laboratory of Physical Chemistry for Solid Surface.

§ Academia Sinica.

10.1021/jp0722105 CCC: $40.75
Published on Web 01/24/2008

neutral water clusters, $(H_2O)_n$, $n = 1-5$ and 8, at the Hartree−Fock level with a basis set of 4-31G. It was found that using larger basis sets made only a small improvement in predicting the Raman intensities of the neutral water clusters.[46−48] Neumann et al. simulated the resonance Raman spectra of the hydrated electron by using the model complexes of the hydronium-water clusters $[H_3O(H_2O)_{3n}$, $n = 0-3]$.[51] Their calculated spectra of the larger clusters (H_3OW_6 and H_3OW_9) were in qualitative agreement with the experiment.[17] Further study is, however, much needed to gain a better understanding of how the hydrogen bonding interactions between water and the related species change the relative Raman intensities.

The goal of the present work is to explore the relationship between the binding interactions and the Raman intensities of the intramolecular modes of water in three H-bonded systems, i.e., the negatively charged water clusters ($(H_2O)_n^-$, $n = 2$ and 3), the water···halide anions ($H_2O\cdots X^-$, X = F, Cl, Br, and I), and the water-metal atom anionic complexes ($H_2O\cdots M^-$, M = Cu, Ag, and Au). Ab initio electronic-structure method (MP2) and density functional theory (DFT) method (B3LYP[52]) are employed. Our results demonstrate that the strong polarization effect of the proton acceptor (X^-, M^-, O, or e^-) contributes to the significant enhancement in the Raman intensities of the H−O−H bending mode of water.

Computational Details

Three kinds of systems have been studied in the present work. They are (1) $(H_2O)_n^-$, where $n = 2$ and 3; (2) $H_2O\cdots X^-$ (X = F, Cl, Br, and I); and (3) $H_2O\cdots M^-$ (M = Cu, Ag, and Au). In order to examine the anionic effect on the change of the Raman intensities, we also calculated the corresponding neutral complexes of systems (1) and (3). Both MP2 and DFT calculations at the level of B3LYP[52] were performed to optimize the geometries and to compute the harmonic vibrational frequencies and the corresponding Raman intensities by using Gaussian 03.[53] The LanL2DZ basis sets were used for the Cu, Ag, and Au atoms, where the relativistic effects were introduced in the effective core potentials for the latter two metals.[54] For the H, O, F, Cl, and Br atoms, we used the augmented Dunning's correlation consistent basis sets of aug-cc-pVTZ (AVTZ).[55] For the I atom, a triple-ζ valence basis set with the pseudopotential (SBK CEP-121) was employed.[56] The validity of these basis sets has been demonstrated in the calculations of water and its coordination complexes with the coinage metals.[39] To ensure a good quality of the basis sets for the water molecule, some calculations were also performed with aug-cc-pVQZ (AVQZ) and aug-cc-pV5Z (AV5Z) for the H and O atoms. The counterpoise method was used to remove the basis set superposition error (BSSE) in calculating the interaction energies.[57,58] Charge distributions were calculated by using the natural bonding orbital (NBO) method.[59]

On the basis of the vibrational frequency analysis, we obtained a force constant matrix of each optimized structure in the Cartesian coordinates. Then the scaled quantum mechanical force field (SQMF) procedure was used to make normal-mode analysis.[60] The procedure can effectively correct the defect of a theoretical method, the basis set limitation, and the anharmonic effect, so that it can properly reproduce the experimental frequencies. The force constants in the Cartesian coordinates were first transformed to those of the internal coordinates. The scaled factors used in the SQMF procedure were obtained by comparing the calculated values to the experimental data for the isolated water. For $H_2O\cdots X^-$, their internal coordinates (S_i, $i = 1-6$) were defined as $S_1 = R(H_b\cdots X)$, $S_2 = \alpha(X\cdots H_b\text{-}O)$, $S_3 = \tau(H_f\text{-}O-H_b\cdots X)$, $S_4 = \alpha(H-O-H)$, $S_5 = R(O-H_b)$, and $S_6 = R(O-H_f)$, respectively. Here, the subscript symbols of b and f denote the hydrogen atom in water, involved (b for bonding) and not involved (f for free) in the hydrogen bonding (HB), respectively. We will call the former the HB O−H bond and the latter the free O−H bond. Similar coordinates were defined for $H_2O\cdots M^-$. The related vibrational modes were denoted as υ_n ($n = 1-6$). We note that, for the $(H_2O)_n^-$ clusters, there exist the HB bonds of the O−H···O type. The "free" O−H bonds may be directed toward the excess electron, forming the HB bonds of the O−H···e^- type.

After carrying out the SQMF calculations, we obtained the scaled vibrational frequencies and the potential energy distribution (PED) of various normal coordinates. This information helped to assign the vibrational frequencies and to analyze the contribution of the internal coordinates to the normal modes. From the normal-mode analysis, we also obtained the transformation matrixes, A and L_S.[61,62] The two matrixes were defined by using the following equations, $X = BR$, $AB = E$, $A = M^{-1}B^TG^{-1}$, and $Q = L_SR$, where B and L_S are the transformation matrixes from displacements of the Cartesian coordinates (X) to the symmetric internal coordinates (R) with respect to their equilibrium positions, and from R to the normal coordinates (Q), respectively. The product E of A and B is the identity matrix. The matrix A was calculated from the matrixes M, B, and G in the normal coordinate analysis, where M is the mass matrix and G is the so-called G matrix in the Wilson GF method.[63] The B^T matrix is a transpose matrix of B. Thus, the atomic polarizability derivative tensor (PD_X) in the Cartesian coordinates can be further converted to the polarizability derivative tensor (PD_Q) in the frame of the normal coordinates by using the expression[62]

$$PD_Q = PD_X A L_S \tag{1}$$

The off-resonance Raman intensity of a given vibrational mode may be calculated as[64,65]

$$I_i^R = \frac{h}{8\pi^2 c\tilde{\nu}_i} \cdot \frac{(\tilde{\nu}_0 - \tilde{\nu}_i)^4}{45[1 - \exp(-hc\tilde{\nu}_i/k_BT)]} (45\bar{\alpha}_i'^2 + 7\gamma_i'^2) \tag{2}$$

where

$$\bar{\alpha}_i' = \frac{1}{3}(PD_{Q,i}^{XX} + PD_{Q,i}^{YY} + PD_{Q,i}^{ZZ}) \tag{3}$$

$$\gamma_i'^2 = \frac{1}{2}[(PD_{Q,i}^{XX} - PD_{Q,i}^{YY})^2 + (PD_{Q,i}^{XX} - PD_{Q,i}^{YY})^2 + (PD_{Q,i}^{XX} - PD_{Q,i}^{YY})^2] + 3[(PD_{Q,i}^{YX})^2 + (PD_{Q,i}^{ZX})^2 + (PD_{Q,i}^{ZY})^2] \tag{4}$$

Here $\tilde{\nu}_0$ and $\tilde{\nu}_i$ denote the frequency of the incident light and the vibrational frequency of the ith mode, respectively.

The Raman scattering factor in the last parenthesis in eq 2 is the quality actually used in the present work to measure the Raman intensity. It contains two contributions: one is from the mean polarizability derivative tensor, $\bar{\alpha}_i'$, and the other is the anisotropic polarizability derivative, $\gamma_i'^2$, of the ith vibrational mode. Since the change of vibrational frequencies is relatively small, the Raman scattering factor is generally used here for comparison of the influence of the binding interaction on the Raman spectral intensities. Here, the enhancement factor will be used to describe the intensity change, which is defined as a

TABLE 1: Calculated Vibrational Frequencies (cm^{-1}), and Theoretical Raman Intensities (I_R in $Å^4$/amu)[a]

	frequency		Raman intensity I_R					
methods	B3LYP[b]	expt.[c]	B3LYP	B3LYP	B3LYP	MP2	CCSD[d]	expt.[c]
basis set	AVTZ		AVTZ	AVQZ	AVQZ	AVTZ		
υ_b	1596.1	1594.7	1.0	0.81	0.76	1.1	1.0	0.9 ± 2
υ_s	3657.1	3657.1	101.3	102.1	102.6	106.3	111	108 ± 14
υ_{as}	3756.0	3755.9	26.5	26.1	26.1	22.8	26.	19.2 ± 2.1

[a] The corresponding experimental data are listed for comparison. [b] The vibrational frequencies are scaled by using the SQMF procedure. Assignments of the vibrational modes are: υ_b, the H−O−H bending mode; υ_s, the symmetric O−H stretching mode; and υ_{as}, the asymmetric O−H stretching mode. [c] The observed vibrational frequencies and Raman intensities are extracted from refs 67 and 68, respectively. [d] From ref 35.

TABLE 2: Calculated Vibrational Frequencies (cm^{-1}) and Raman Intensities (I_R in $Å^4$/amu) of $(H_2O)_2$ and $(H_2O)_2^-$

	neutral				anion				
methods	B3LYP			MP2	B3LYP				MP2
basis set	AVTZ	AVTZ	AVQZ	AVTZ	AVZ	AVTZ	AVQZ	AV5Z	AVTZ
modes	freq[a]	I_R	I_R	I_R	freq[a]	I_R	I_R	I_R	I_R
$\upsilon_{b,a}$	1597.6	1.0	0.9	1.1	1543.9	52088.0	141740.6	334243.4	257190.4
$\upsilon_{b,d}$	1618.5	0.7	0.7	0.6	1633.8	99077.3	140827.6	119226.2	27022.4
$\upsilon_{s,db}$	3538.2	164.8	166.5	163.4	3378.0	410975.3	467835.3	1174113.0	725804.6
$\upsilon_{s,a1f}$	3649.3	83.8	83.9	81.0	3448.3	102131.8	132377.2	547169.9	439576.2
$\upsilon_{s,df}$	3726.8	49.8	49.8	42.9	3647.7	11313.1	13738.1	31023.8	223515.0
$\upsilon_{s,a2f}$	3745.9	25.1	24.9	21.7	3485.4	26451.5	89863.9	17333.6	34533.6

[a] Vibrational frequencies calculated at B3LYP/AVTZ are scaled using the SQMF procedure. Assignments of the vibrational modes are: $\upsilon_{b,a}$ and $\upsilon_{b,d}$, the H−O−H bending modes of the proton-acceptor water and the proton-donor water, respectively; $\upsilon_{s,db}$ and $\upsilon_{s,df}$, the HB O−H stretching mode and the free O−H stretching mode, respectively, for the proton-donor water; $\upsilon_{s,a1f}$ and $\upsilon_{s,a2f}$, the free O−H stretching modes for the proton-acceptor water.

ratio of the Raman scattering factors of the same vibrational mode in water anionic complexes and the free water molecule.

Results and Discussion

Bare Water. To study the influence of the hydrogen bonding on the Raman spectra, we selected the free water molecule as the reference. Its fundamental spectral parameters are first discussed here. The validity of the theoretical method at the present level of B3LYP/AVTZ is examined by predicting structures and the Raman spectra of a free water molecule. The bond distance and the bond angle were predicted to be 0.962 Å and 105.4°, respectively, in good agreement with the experimental values of 0.959 Å and 104.45°.[66] It is well-known that the water molecule has three normal modes, i.e., the bending mode (υ_b: a_1), the symmetric stretching mode (υ_s: a_1), and the asymmetric stretching mode (υ_{as}: b_2). The harmonic fundamentals are predicted to be 1627.6, 3795.7, and 3898.3 cm^{-1}, respectively. They can be scaled to 1596.1, 3657.1, and 3756.0 cm^{-1}, respectively, by using the SQMF procedure. These numbers agree well with the experimental frequencies, 1594.7, 3657.1, and 3755.9 cm^{-1}.[67] Two scaling factors have been used, which are 0.927 for the B3LYP/AVTZ force constants of the O−H stretching coordinates and 0.963 for that of the H−O−H bending coordinate. These two scaling factors will be used to calculate the scaled frequencies for various water complexes studied in the next section. The SQMF scaled vibrational frequencies are not very sensitive to the theoretical methods, so only values of B3LYP/AVTZ will be reported for all complexes studied in the present work.

We calculated the Raman intensities with MP2 and B3LYP by using the AVTZ basis set, and compared the results with those of CCSD in the literature[35] (see Table 1). The Raman intensities for three modes calculated by MP2 and CCSD are 1.1, 105.3, and 22.4 $Å^4$/amu and 1.0, 111, and 26 $Å^4$/amu, respectively. These values agree well with the experimental data of 0.9 ± 2, 108 ± 14, and 19.2 ± 2.1 $Å^4$/amu for the corresponding normal modes.[68,69] B3LYP/AVTZ also gives satisfactory results. The predicted Raman intensities are 1.0 (υ_b), 101.3(υ_s), and 26.5 $Å^4$/amu (υ_{as}). As seen from Table 1, increasing the size of the basis sets from AVTZ to AV5Z leads to only a small improvement in predicting the Raman intensities of the water molecule. This reveals that the B3LYP/AVTZ method is sufficient to obtain the converged Raman intensities for an isolated water molecule, although, as we will show below, such a level may not be good enough for a quantitative description of an anionic complex. Recently, the DFT method (B3LYP/6-311+G**) has been used to analyze the binding interaction and the Raman intensities in the H-bonded complexes and the coinage metal-pyridine clusters.[70] This success encourages us to explore the bonding effect on the vibrational Raman intensities of the hydrogen-bonded anionic complexes.

Anionic Water Clusters $(H_2O)_n^-$, $n = 2$ and 3. The hydrated electron in the small anionic water clusters is usually considered to be dipole bound, showing that the excess electron populates the highest occupied molecular orbital (HOMO) localized at the positive end of the cluster dipole moment.[37] This configuration significantly enhances the infrared intensities of the water molecule close to the dipole-bound electron. It is also expected to enhance the Raman intensities of such water. Table 2 presents our calculated vibrational frequencies and Raman intensities of the water dimer complexes. In order to see clearly the origin of the difference in the Raman spectra between $(H_2O)_2$ and $(H_2O)_2^-$, it is necessary to examine first their geometric difference (see Figure 1). For $(H_2O)_2$, the free O−H bonds adopt an anti configuration[48,36,71−74] as the free O−H of the proton-donor water is on the other side of the two O−H bonds of the proton-acceptor water along the axis of the hydrogen bond (Figure 1a). For $(H_2O)_2^-$, it has to adopt a cis configuration with all free O−H bonds on the same side (Figure 1b). Such a configuration has a larger dipole moment to stabilize the excess electron.[36,71] The electron density plot of HOMO presented in Figure 1c shows that the excess electron is mainly localized in the region near two free O−H bonds of the proton-acceptor water. Hence, for the neutral water dimer, the lowest

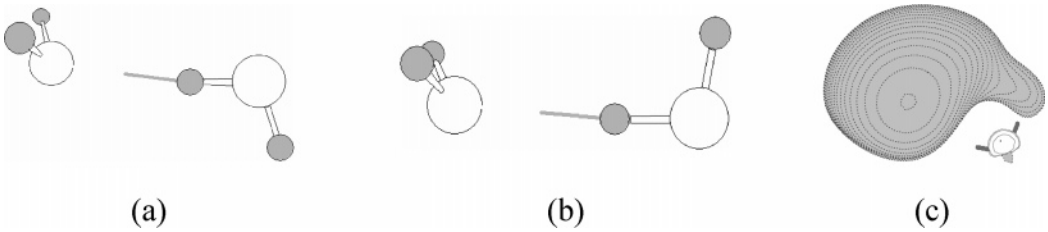

Figure 1. Optimized geometries of (a) $(H_2O)_2$ and (b) $(H_2O)_2^-$ at the level of B3LYP/AVTZ. (c) The electron density plot of the highest occupied molecular orbital (HOMO) of $(H_2O)_2^-$.

TABLE 3: Calculated Vibrational Frequencies (cm^{-1}) and Raman Intensities (I_R in $Å^4$/amu) of $(H_2O)_3$ and $(H_2O)_3^-$

	neutral				anion			
method	B3LYP			MP2	B3LYP			MP2
basis set	AVTZ	AVTZ	AVQZ	AVTZ	AVTZ	AVTZ	AVQZ	AVTZ
mode	freq[a]	I_R	I_R	I_R	freq	I_R	I_R	I_R
$\upsilon_{b,1}$	1608.0	1.2	1.1	1.1	1594.0	18125.7	18591.6	20988.4
$\upsilon_{b,2}$	1610.1	1.1	1.1	1.3	1594.0	15867.5	23182.3	21258.0
$\upsilon_{b,3}$	1633.7	1.3	1.2	1.1	1617.2	106774.6	136933.0	214875.8
$\upsilon_{s,1b}$	3394.7	268.2	266.8	276.2	3375.0	33450.1	47452.4	29132.1
$\upsilon_{s,2b}$	3457.1	34.0	34.4	27.6	3430.5	23138.9	22913.4	68332.3
$\upsilon_{s,3b}$	3468.1	34.7	33.9	26.8	3431.2	23799.5	23101.3	55081.3
$\upsilon_{s,1f}$	3720.7	52.5	51.6	47.8	3549.3	25700.9	25506.8	236198.6
$\upsilon_{s,2f}$	3724.6	42.1	40.3	44.1	3549.5	25880.0	26122.5	183908.3
$\upsilon_{s,3f}$	3725.8	99.1	99.8	76.7	3572.2	128495.0	222604.8	70502.4

[a] Vibrational frequencies calculated at B3LYP/AVTZ are scaled using the SQMF procedure. Assignments of the vibrational modes are: $\upsilon_{b,i}$ ($i = 1-3$), the H−O−H bending modes; $\upsilon_{s,ib}$ ($i = 1-3$), the HB O−H stretching modes; and $\upsilon_{s,if}$ ($i = 1-3$), the free O−H stretching modes.

O−H stretching frequency ($\upsilon_{s,db}$) has the strongest Raman intensity. Its Raman intensity is enhanced by about 1.6 times over that in a water monomer. This is in agreement with the previous Hartree−Fock predictions[46,47] and the experimental observation.[75] The $\upsilon_{s,db}$ peak, showing a scaled frequency of 3538.2 cm^{-1}, can be assigned to the HB O−H stretching vibration of the proton-donor water. There is a red-shift of about 119 cm^{-1} with respect to 3657 cm^{-1} in the free water molecule.[67] The predicted frequency is too low as compared to 3601 cm^{-1} observed for a water dimer,[76] indicating an accurate force constant of this normal mode is important.[74] However, the vibrational frequencies are very sensitive to the matrix effect that may give rise to the intermolecular interactions strong enough to change the equilibrium structure of the water clusters.[76] Hence, the experiment did not provide a clear-cut situation, with which the theory can make unambiguous comparison. For the two bending modes, the Raman intensities are about 1.0 $Å^4$/amu, close to that of the free water molecule. As seen in Table 2, the B3LYP results are in good agreement with the MP2 results, supporting that the DFT calculations at this level can predict well the Raman intensities of the neutral water dimer.

The anionic dimer, $(H_2O)_2^-$, not only has a significant red-shift of the vibrational frequencies for all its four O−H stretching modes but also exhibits a marked enhancement in their Raman intensities. As seen in Table 2, the lowest frequency of the O−H stretching vibration has the strongest Raman signal. This frequency can also be attributed to the HB O−H stretching vibration of the proton-donor water ($\upsilon_{s,db}$). The symmetric O−H stretching vibration ($\upsilon_{s,a1f}$) in the proton-acceptor water is the second strongest in terms of the Raman intensity.

The dipole-bound electron also leads to a significant red-shift of the bending mode ($\upsilon_{b,a}$) of the proton-acceptor water molecule to 1543.9 cm^{-1}, as compared to that (1593 cm^{-1}) of the free water molecule. The predicted frequency of $\upsilon_{b,a}$ is closer to the observed frequencies from the infrared measurements, such as 1535 cm^{-1} in $(H_2O)_8^-$.[37,77] Interesting, we note that the bending frequency ($\upsilon_{b,d}$) of the proton-donor water significantly blue-shifts to 1633.8 cm^{-1}. For both bending modes, there is a significant enhancement in the Raman intensities as compared to those of the neutral water dimer.

Adding an excess electron causes the enhancement of the Raman intensities by about 10^4 folds for the $\upsilon_{s,db}$ mode and about 10^5 folds for the $\upsilon_{b,a}$ mode. The ratio of the Raman intensities between the strongest H−O−H bending mode and the strongest O−H stretching mode in $(H_2O)_2^-$ are between 0.28 and 0.30 at B3LYP with different basis sets, whereas that from the MP2/AVTZ is 0.35. These are one magnitude larger than 0.01 found in H_2O and $(H_2O)_2$. However, it is difficult to directly compare the absolute Raman intensity calculated by using the B3LYP method and those from the MP2 method. The calculated Raman intensities strongly depend on the basis set and the theoretical method for the $(H_2O)_2^-$ cluster (see Table 2).

Table 3 presents the calculated vibrational frequencies and the corresponding Raman intensities of the water trimer complexes. The most stable configurations are shown in Figure 2. For $(H_2O)_3$, one of three free O−H bonds adopts an anti configuration. The lower O−H stretching frequencies are associated with the HB O−H bonds, whereas the higher O−H stretching frequencies are associated with the free O−H bonds. Both B3LYP and MP2 methods conclude that it is the lowest O−H stretching frequency ($\upsilon_{s,1b}$) that has the largest Raman intensity (268.2 $Å^4$/amu for B3LYP and 276.2 $Å^4$/amu for MP2 with the AVTZ basis set). For $(H_2O)_3^-$, all three free O−H bonds adopt a cis configuration, maximizing its dipole moment to stabilize the excess electron.[37] The electron density distribution of HOMO plotted in Figure 2c shows that the three free O−H groups are directed toward the excess electron. This results in the strongest Raman intensity associated with the free O−H stretching mode. As seen in Table 3, although B3LYP predicts that the highest O−H stretching frequency has the strongest Raman signal, MP2 predicts that the strongest Raman signal comes from two near degenerate modes of the free O−H stretching vibrations. This discrepancy between two theoretical

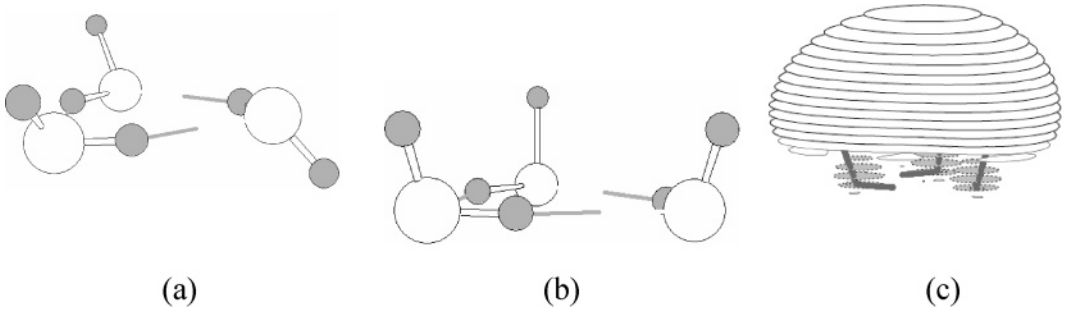

Figure 2. Optimized geometries of (a) $(H_2O)_3$ and (b) $(H_2O)_3^-$ at the level of B3LYP/AVTZ. (c) The electron density plot of the highest occupied molecular orbital (HOMO) of $(H_2O)_3^-$.

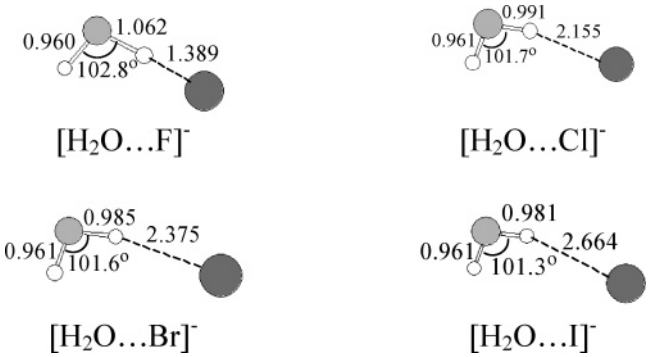

Figure 3. Optimized geometries of $H_2O\cdots X^-$ (X = F, Cl, Br, and I) at the level of B3LYP/AVTZ. The basis set for I is SBK CEP-121.

methods reflects a different response for the free O−H stretching vibrations to the polarization of the dipole-bound electron. Nevertheless, both methods conclude that the ratio of Raman intensities between the strongest bending mode and the strongest O−H stretching mode increase to 0.62 for B3LYP/AVQZ and 0.91 for MP2/AVTZ, as compared to 0.01 in the free water molecule.

Water−Halide Anionic Complexes. Figure 3 shows the equilibrium geometries of the water-halide (F^-, Cl^-, Br^-, and I^-) complexes. All of these complexes exhibit an asymmetric structure, in agreement with previous studies.[29−33] The binding energies (BE) are calculated according to $BE = -[E(H_2O\cdots X^-) - E(H_2O) - E(X^-)]$, where X^- denotes a halide anion. The binding energy in $H_2O\cdots F^-$ is predicted to be 27.3 kcal/mol, which is almost twice as large as the values of 14.2 kcal/mol for $H_2O\cdots Cl^-$, 11.1 kcal/mol for $H_2O\cdots Br^-$, and 11.6 kcal/mol for $H_2O\cdots I^-$. After the corrections of the BSSE effect, these binding energies become 27.1, 14.1, 11.0, and 10.6 kcal/mol, respectively. These corrected values are in good agreement with the measured disassociation energies of 26.2, 14.9, 11.7, and 10.3 kcal/mol for H_2O interacting with F^-, Cl^-, Br^-, and I^-, respectively.[30] NBO analysis suggests that the interaction increases the electron occupancy in the antibonding orbital of the HB O−H bond. This will lead to a red-shift of the vibrational frequencies for the HB O−H stretching mode of $H_2O\cdots X^-$.

Table 4 presents the scaled vibrational frequencies and the corresponding Raman intensities for $H_fOH_b\cdots X^-$. The results show that the HB O−H stretching frequencies (υ_5) blue-shift with the increasing size of the halide ions.[30−33,71] The scaled vibrational frequencies of the υ_5 mode at the present theoretical level are 2058.4 (F^-), 3175.3 (Cl^-), 3288.4 (Br^-), and 3367.3 cm^{-1} (I^-), respectively. The observed frequencies of the υ_5 vibration are 1523 (F^-), 3130 (Cl^-), 3267 (Br^-), and 3295 cm^{-1} (I^-) cm^{-1}.[30,72−74] The significant difference between the experimental and theoretical frequencies in $H_2O\cdots F^-$ is mainly due to a large anharmonic effect for the $O-H\cdots F^-$ hydrogen bond.[45b,78] On the other hand, the free O−H stretching (υ_6) frequencies in the four complexes are all around 3700 cm^{-1}, in agreement with the IR spectral peaks observed at 3690 ($H_2O\cdots F^-$), 3698 ($H_2O\cdots Cl^-$), 3690 ($H_2O\cdots Br^-$), and 3710 cm^{-1} ($H_2O\cdots I^-$).[30] Our normal-mode analysis shows that the υ_5 and υ_6 modes are uncoupled. The contribution of the PED values of each O−H stretching coordinate to the respective vibrational mode is no less than 98%. Among the six fundamentals, the $H_b\cdots X$ stretching mode (υ_1) has the lowest vibrational frequency. The calculated trend in the υ_1 frequencies from F^- to I^- is in accordance with the experimental observations.[30,79] Experimentally, the υ_1 peaks were observed at 210 (Cl^-), 158 (Br^-), and 135 (I^-) cm^{-1} for the $H_2O\cdots X^-$ clusters in the gas phase,[30] and 252 (F^-), 185 (Cl^-), 175 (Br^-), and 150 (I^-) cm^{-1} in the aqueous solutions.[79] Our calculated numbers are 392.3 (F^-), 191.0 (Cl^-), 157.8 (Br^-), and 124.6 (I^-) cm^{-1}.

TABLE 4: Vibrational Frequencies (cm^{-1}) and Raman Intensities (I_R in $Å^4$/amu) of $H_2O\cdots X^-$ (X = F, Cl, Br, and I) Calculated at the B3LYP/AVTZ Level[a]

	$H_2O\cdots F^-$		$H_2O\cdots Cl^-$		$H_2O\cdots Br^-$		$H_2O\cdots I^-$	
mode	freq[b]	I_R	freq[b]	I_R	freq[b]	I_R	freq[b]	I_R
υ_1	392.3	0.2	191.0	0.9	157.8	1.3	124.6	2.9
υ_2	570.0	2.1	359.0	2.2	314.3	2.0	250.1	26.3
υ_3	1144.1	4.8	729.2	6.9	658.6	7.9	603.3	104.0
υ_4	1668.4	1.7	1639.1	3.7	1634.1	5.9	1629.2	47.2
υ_5	2058.4	0.2	3175.3	222.8	3288.4	271.5	3367.3	477.2
υ_6	3704.3	87.8	3711.3	69.1	3709.7	70.9	3704.9	61.5

[a] The basis set for I is SBK CEP-121. [b] Assignments of the vibrational modes are: υ_1, the $H_b\cdots X$ stretching; υ_2, the $O-H_b\cdots X$ bending; υ_3, the $H_f-O-H_b\cdots X$ torsion; υ_4, the H−O−H bending; υ_5, the $O-H_b$ stretching; and υ_6, the $O-H_f$ stretching. X, b, and f denote a halide ion, the hydrogen-bonded proton and the free hydrogen atom in water, respectively.

The results presented in Table 4 show that the Raman intensities of the υ_5 (the $O-H_b$ stretching) and υ_4 (the H−O−H bending) modes increase in the order of $F^- < Cl^- < Br^- < I^-$. The effect of charge transfer from the halide anions to the solvent water molecules was believed to play an important role in infrared spectral intensities of water.[30−33] However, from the NBO analysis, we obtain the net transferred charges from halides to the water molecule are 0.130 (F^-), 0.055 (Cl^-), 0.043 (Br^-), and 0.041e (I^-), respectively, antiparallel to the observed trend of the Raman intensities of υ_5 and υ_4. Hence, such a charge-transfer effect is not anticipated to be significant. We believe that it is the polarization effect that makes the main contribution. The HB proton of the water molecule may polarize the anion, yielding a larger induced dipole moment at a less polar O−H bond.[8] For halide anions, their static polarizabilities increase in the order of $F^- < Cl^- < Br^- < I^-$. One would expect the largest induced dipole moment in the $H_2O\cdots I^-$ complex. In order to quantitatively estimate the polarization effect, we calculate the

TABLE 5: Isotropic Polarizability Derivatives (Å²/amu$^{1/2}$) and Square of Anisotropic Polarizability Derivatives (Å⁴/amu) of the $H_2O\cdots X^-$ Complexes[a]

species	$H_2O\cdots F^-$		$H_2O\cdots Cl^-$		$H_2O\cdots Br^-$		$H_2O\cdots I^-$	
mode[b]	$\bar{\alpha}'$	γ'^2	$\bar{\alpha}'$	γ'^2	$\bar{\alpha}'$	γ'^2	$\bar{\alpha}'$	γ'^2
υ_1	0.03	0.02	0.14	0.00	0.17	0.01	−0.20	0.14
υ_2	0.10	0.23	0.07	0.28	0.03	0.28	0.34	3.01
υ_3	0.00	0.68	0.00	0.99	0.00	1.13	0.00	14.84
υ_4	0.04	0.26	0.10	0.47	0.18	0.64	−0.42	5.67
υ_5	0.93	3.76	1.18	22.84	1.18	29.76	2.45	29.38
υ_6	1.17	3.80	1.08	2.39	1.11	2.15	0.91	3.49

[a] Calculated at the B3LYP/AVTZ level. [b] Please refer to Table 4 for the assignments of the vibrational modes.

isotropic and anisotropic polarizability derivatives with respect to the normal coordinates by using eqs 3 and 4. The results are summarized in Table 5.

For the υ_5 mode, Table 5 shows that the hydrogen bonding interaction results in an increase in the anisotropic polarizability derivatives with the increasing size of halides, i.e., 3.76 (F^-), 22.84 (Cl^-), 29.76 (Br^-), and 29.38 Å⁴/amu (I^-). For this mode, the isotropic polarizability derivatives are around 1 Å²/amu$^{1/2}$ for X = F, Cl, and Br. It is more than doubled to 2.5 Å²/amu$^{1/2}$ for X = I (see Table 5). Clearly, it is the anisotropic polarizability derivative that makes the Raman intensity of the υ_5 mode larger for X = Cl, Br, and I than for X = F, whereas it is the isotropic polarizability derivative that makes the Raman intensity of this mode larger for X = I than for X = F, Cl, and Br. Hence, by combining these two polarization effects, we have the calculated Raman intensities which follow the trend of I_R (0.2, F^-) ≪ I_R (222.8, Cl^-) < I_R (271.5, Br^-) < I_R (477.2, I^-) (see Table 4).

With respect to the free water, the enhancement factors in the Raman intensities of the υ_5 (the $O-H_b$ stretching) mode are estimated to be about 2 (Cl^-), 2.4 (Br^-), and 4.3 (I^-). The calculated values are slightly larger than the ones (1.1, 1.8, and 1.7) observed from the corresponding halide electrolyte solutions for Cl^-, Br^-, and I^-, respectively.[7] Such a difference is understandable, since the polarizabilities of these halide anions are sensitive to the change of their chemical environments. For example, the polarizabilities of the halide anions in vacuum predicted from the B3LYP calculations are 3.39 for F^-, 6.33 for Cl^-, 8.18 for Br^-, and 11.19 Å³ for I^-.[80] However, the polarizabilities are reduced, as expected. A compression of the electron density in bulk solutions results from the polarization and electrostatic repulsion effects from other ions in solutions.[80] In ionic crystals, the experimental polarizabilities of these halide anions further decrease to about 1.04, 3.66, 4.77, and 7.1 Å³ for F^-, Cl^-, Br^-, and I^-, respectively.[81,82] Therefore, we conclude that addition of a salt with large polarizability anions will lead to an enhancement in the Raman signal of the solvent water molecules in the first solvated shell. The present results are well supported by recently reported Raman spectra.[11,12]

The Raman intensity of the bending mode (υ_4) of water is also found to strongly depend on the property of the halide anions. As shown in Table 4, υ_4 in $H_2O\cdots I^-$ exhibits the strongest Raman intensity. On the basis of Raman spectra of alkali halide aqueous solutions, Schultz and Hornig obtained enhancement factors of 0.5, 1.9, 7.8, and 10.9 for F^-, Cl^-, Br^-, and I^-, respectively,[7] which are in agreement with our present results, i.e., 1.7, 3.7, 5.9, and 47.2. The data listed in Table 5 show that for the H−O−H bending mode, both the isotropic and anisotropic polarizability derivatives increase in magnitude from F^- to I^-. In particular, a significant increase takes place in the anisotropic part from Br^- to I^- (i.e., from 0.64 to 5.67 Å⁴/amu). Detailed analysis of the polarizability derivatives of the anisotropic part show that this jump comes from an increase in the polarizability derivative of α'_{yx}, to which the main contributions are from the two bending coordinates, S_4 (H−O−H) and S_2 ($X\cdots H_b$-O). Hence, we may decompose the anisotropic polarizability derivatives into two parts: 0.09 (S_4) + 0.17 (S_2) = 0.26 (F^-), 0.09 + 0.37 = 0.46 (Cl^-), 0.12 + 0.52 = 0.64 (Br^-), and 0.77 + 4.90 = 5.67 Å⁴/amu (I^-). According to eq 2, the contributions to the total Raman intensities of the H−O−H bending mode from the isotropic versus anisotropic parts of only S_4 and S_2 are 0.06 vs 1.81, 0.43 vs 3.26, 1.46 vs 4.47, and 8.00 vs 39.67 Å⁴/amu in $H_2O\cdots X^-$ for $X = F^-$, Cl^-, Br^-, and I^-, respectively. It suggests that such an enhancement could be interpreted by the vibrational coupling between the H−O−H and $X\cdots H_b$-O bending coordinates. The former borrows the polarizability derivative from the latter. The HB bonding interaction plays an important role in the enhancement of the Raman intensity of the H−O−H bending mode in the $H_2O\cdots I^-$ complex.

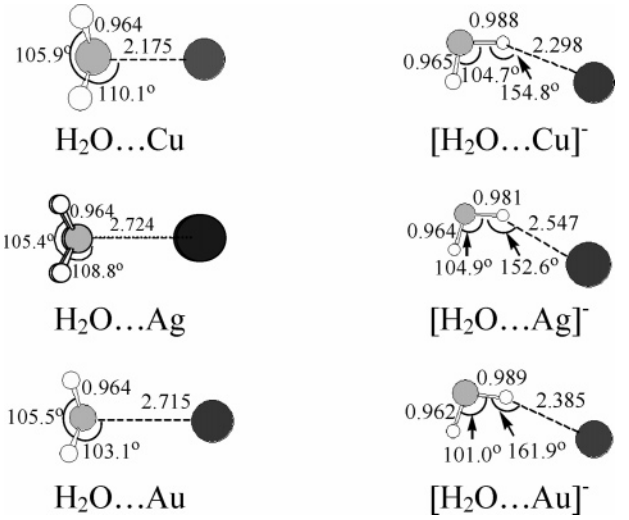

Figure 4. Optimized geometries of $H_2O\cdots M^\delta$ (M = Cu, Ag, and Au, δ = 0 and −1) at the level of B3LYP/AVTZ(O,H)/Lanl2DZ(M).

$H_2O\cdots M^-$ Anionic Complexes. Figure 4 shows the optimized structures for $(H_2O\cdots M)^\delta$ (δ = 0 and −1). The neutral complexes adopt an O-end configuration. The calculated binding energies are 7.25, 2.13, and 2.61 kcal/mol for M = Cu, Ag, and Au, respectively. After the BSSE corrections, the corresponding binding energies decrease to 4.93, 1.05, and 1.60 kcal/mol. The anionic complexes adopt an H-end configuration, where the water−metal interaction is significantly strengthened. The calculated binding energies are 20.80, 14.78, and 14.32 kcal/mol for the Cu, Ag, and Au anionic complexes, respectively. After the BSSE corrections, the corresponding binding energies are 10.45, 9.61, and 11.36 kcal/mol, respectively. The BSSE effect is most severe in $H_2O\cdots Cu^-$, signifying that the LanL2DZ basis set for Cu may be problematic. The BSSE-corrected B3LYP binding energies are in good agreement with 10.61[41] and 11.28 kcal/mol[43] for $H_2O\cdots Cu^-$, 10.33[43] for $H_2O\cdots Ag^-$, and 12.43 kcal/mol for $H_2O\cdots Au^-$ [43] at the CCSD(T) level reported in literatures. Our results support that the binding interactions are indeed stronger in $H_2O\cdots M^-$ than those in $H_2O\cdots M$.[3940−43,83]

The calculated vibrational frequencies and Raman intensities are presented in Table 6 for $H_2O\cdots M$ and Table 7 for $H_2O\cdots M^-$. According to the analysis of the scaled vibrational frequencies, we may draw the following two conclusions. First, the interaction of a metal atom with the oxygen atom of water leads to a

TABLE 6: Calculated Vibrational Frequencies (cm^{-1}) and Raman Intensities (I_R in $Å^4$/amu) of the $H_2O\cdots M$ (M = Cu, Ag, and Au) Complexes

	frequencies	Raman intensity I_R			
method		B3LYP			MP2
basis set	AVTZ	AVTZ	AVQZ	AV5Z	AVTZ
$H_2O\cdots Cu$					
υ_1	200.3	117.6	135.9	137.4	193.8
υ_2	327.1	175.9	169.0	167.9	102.9
υ_3	368.3	20.7	22.9	26.1	204.7
υ_4[b]	1572.2	188.4	208.3	213.6	211.4
υ_5	3566.2	2389.3	2602.9	2754.2	9887.6
υ_6	3669.1	307.8	345.8	365.3	366.6
$H_2O\cdots Ag$					
υ_1	103.0	15.7	15.7	17.4	54.7
υ_2	212.0	19.3	19.3	11.9	57.5
υ_3	230.8	9.7	10.9	17.7	108.3
υ_4	1584.1	19.8	19.4	20.5	35.3
υ_5	3624.3	693.3	699.9	734.9	1759.4
υ_6	3726.2	65.9	62.9	64.0	78.4
$H_2O\cdots Au$					
υ_1	105.2	1.7	2.1	3.1	3.4
υ_2	281.1	2.4	1.9	1.5	13.1
υ_3	299.6	1.2	1.40	1.8	10.16
υ_4	1582.8	3.7	4.16	4.3	16.2
υ_5	3629.9	235.0	247.9	285.7	435.5
υ_6	3730.9	30.8	31.0	33.8	31.6

[a] Symmetric coordinates were defined as, $s_1 = (r_1 + r_2)/\sqrt{2}$, $s_2 = (r_1 - r_2)/\sqrt{2}$, $s_3 = R$, $s_4 = (2\alpha - \beta_1 + \beta_2)/\sqrt{6}$, $s_5 = (\beta_1 - \beta_2)/\sqrt{2}$, $s_6 = \gamma$. Here, r_1, r_2, R, α, β_1, β_2, and γ denote the internal coordinators of O_1H_2, O_1H_3, and OM bond stretches, $H_2O_1H_3$, $H_2O_1M_4$, $H_3O_1M_4$ angle bending coordinators, the out-of-plane bending angle of Cu with respect to the H_2O plane, respectively. The assignments are: υ_1, Au$\cdots$OH$_2$ stretching; υ_2, Out-of-plane bending; υ_3 H_2O wag; υ_4, H−O−H bending; υ_5 Symm. O−H stretching; υ_6, Asymm. O−H stretching. [b] Experimental value in ref 84 for the H−O−H bending mode in $H_2O\cdots Cu$ is 1572.8 cm^{-1}.

TABLE 7: Calculated Vibrational Frequencies (cm^{-1}), and Raman Intensities (I_R in $Å^4$/amu) of the $H_2O\cdots M^-$ (M = Cu, Ag, and Au) Complexes[a]

	freq[b]	Raman intensity I_R			
methods		B3LYP			MP2
basis set	AVTZ	AVTZ	AVQZ	AV5Z	AVTZ
$H_2O\cdots Cu^-$					
υ_1	112.9	55.3	32.8	54.2	50.9
υ_2	233.0	148.5	141.8	301.5	179.2
υ_3	541.1	346.0	353.4	335.9	199.2
υ_4	1596.1	3055.7	3486.1	4714.0	2068.7
υ_5	3210.7	4061.7	3690.8	9410.7	21037.5
υ_6	3652.2	1791.1	1697.8	2070.5	2539.7
$H_2O\cdots Ag^-$					
υ_1	105.2	66.5	53.5	60.9	62.0
υ_2	219.0	118.3	118.0	212.9	105.9
υ_3	528.6	254.0	271.9	406.8	225.4
υ_4	1608.5	2301.3	2435.7	3754.5	1180.3
υ_5	3345.5	2100.8	2249.5	4039.1	9495.8
υ_6	3660.7	1748.0	1791.3	1957.7	2574.7
$H_2O\cdots Au^-$					
υ_1	97.0	5.2	2.3	1.4	14.2
υ_2	262.7	9.9	7.4	9.6	1.3
υ_3	610.7	59.9	76.2	114.2	36.9
υ_4	1610.5	130.8	126.8	136.6	57.4
υ_5	3194.5	454.4	483.4	551.2	1295.9
υ_6	3692.2	316.0	312.1	325.9	386.0

[a] Assignments of the vibrational modes are: υ_1, the $H_b\cdots M^-$ stretching; υ_2, the $O-H_b\cdots M^-$ bend; υ_3, the H_f-$O-H_b\cdots M^-$ torsion; υ_4, the H−O−H bend; υ_5, the $O-H_b$ stretch; and υ_6, the $O-H_f$ stretch. M^-, b, and f denote a metal anion, the hydrogen-bonded proton and the free hydrogen atom in water, respectively. [b] Vibrational frequencies calculated at B3LYP/AVTZ are scaled by using the SQMF procedure. The LanL2DZ basis sets are used for Cu, Ag, and Au.

certain red shift for both the O−H stretching modes and the H−O−H bending mode with respect to the fundamentals in the free water. For $H_2O\cdots Cu$, the scaled H−O−H bending frequency (1572.2 cm^{-1}) is in very good agreement with 1572.8 cm^{-1} from an IR experiment,[84] although it is smaller than the previous theoretical predictions for $H_2O\cdots Cu$.[38,41] Vibrational spectra of $H_2O\cdots Ag$ and $H_2O\cdots Au$ clusters are not yet available in the literature. Second, for the $H_2O\cdots M^-$ complexes, the HB interactions cause a red-shift of the υ_5 frequency and a blue shift of the υ_4 frequency. It is worthy to note there is a recent infrared study with Ar photodissociation spectroscopy by Schneider et al.[43] They observed the O−H stretching bands at 3271 and 3520 cm^{-1} for $H_2O\cdots Cu^-$, 3366 and 3575 cm^{-1} for $H_2O\cdots Ag^-$, and 3144 and 3677 cm^{-1} for $H_2O\cdots Au^-$. The largest difference between theory and experiment appears in the υ_6 mode (the free O−H stretching). Although the experiment showed a large frequency difference of 157 cm^{-1} from Cu^- to Au^-, the corresponding difference in theory is only 40 cm^{-1} from our calculations. Since the PED values indicate that the υ_6 mode has almost no coupling with other modes. It is expected that the υ_6 vibrational frequency should have a small difference in all three $H_2O\cdots M^-$ complexes, as seen in the cases of the water−halide anionic complexes.

Now let us focus on the changes of the Raman intensities. Changes of Raman intensities depend on two aspects. First, the enhancements of the Raman intensities for both the O−H stretching mode and the bending mode follow the sequence of $Au^\delta < Ag^\delta < Cu^\delta$ ($\delta = 0$ and -1). This can be interpreted by the polarization effect along this series of the metal atom and its anions. A quality defined to measure the polarization ability of a metal is the ratio of the atomic polarizability over the corresponding atomic volume. We find that Cu^δ has a larger polarizability per volume than Ag^δ and Au^δ. Our B3LYP/LanL2DZ calculations give the polarizabilities of the neutral metal atoms as 7.3 $Å^3$ for Cu, 7.9 $Å^3$ for Ag, and 5.5 $Å^3$ for Au. These are comparable to 6.1, 7.2, and 5.8 $Å^3$ estimated from a relativistic linear response method[82] and 9.3,[3] 14.9,[3] and 7.1 $Å^3$ from the CCSD calculations.[85−89] On the other hand, we calculate the volumes of these three atoms as 104.3, 123.6, and 108.6 $Å^3$, which are defined as volumes inside a counter of 0.001 e/bohr^3 density. This yields the polarizability per volume in the sequence of 0.070, 0.064, and 0.051 for Cu, Ag, and Au, respectively. For the metal anions, the B3LYP polarizabilities increase significantly to 23.6, 22.6, and 10.7 $Å^3$ as compared to the neutral atoms. The corresponding values, 48.6, 42.6, and 18.6 $Å^3$ for Cu^-, Ag^-, and Au^-, respectively,[85−89] from the CCSD calculations are larger but follow the same trend. The volumes, computed at the B3LYP/LanL2DZ level, are 122.4, 138.5, and 130.9 $Å^3$ for Cu^-, Ag^-, and Au^-, respectively. Hence, the calculated polarizabilities per volumes are 0.193 (Cu^-) > 0.163 (Ag^-) > and 0.082 (Au^-). This order is in accord with the largest Raman intensity found in $H_2O\cdots Cu^-$ and the smallest intensity in $H_2O\cdots Au^-$. This suggests that copper, atom or anion, is easier to be polarized than Ag and Au.

Second, addition of an excess electron to the neutral $H_2O\cdots M$ complexes significantly changes the relative Raman intensities between the υ_4 (H−O−H bending) and υ_5 ($O-H_b$ stretching) modes. From Table 7, we calculate, at B3LYP/AVTZ, the smallest I_R (υ_4)/I_R (υ_5) ratio to be 0.29 in $H_2O\cdots Au^-$. The ratios increase to 0.75 and 1.10 for $H_2O\cdots Cu^-$ and $H_2O\cdots Ag^-$, respectively. They are much larger than the experimental value (∼0.01) of the gas-phase water[68] and are also larger than the values between 0.02∼0.08 for $H_2O\cdots M$ and 0.02∼0.1 found in the $H_2O\cdots X^-$ (X = Cl, Br, and I) complexes from the above

TABLE 8: Isotropic Polarizability Derivatives (Å²/amu^1/2) and Square Anisotropic Polarizability Derivatives (Å⁴/amu) of Intramolecular Modes of Water in the $H_2O\cdots M^-$ Complexes[a]

species	$H_2O\cdots Cu^-$		$H_2O\cdots Ag^-$		$H_2O\cdots Au^-$	
mode[a]	$\bar{\alpha}'$	γ'^2	$\bar{\alpha}'$	γ'^2	$\bar{\alpha}'$	γ'^2
υ_4	7.87	39.82	6.76	35.05	1.56	3.09
υ_5	−8.99	57.26	−6.15	55.57	−1.15	56.24
υ_6	4.26	139.47	4.42	124.62	2.25	12.70

[a] Calculated at the B3LYP/AVTZ(H,O) & LanL2DZ(M). [b] Please refer to Table 7 for the assignments of the vibrational modes.

calculations. Even though the quantitative numbers may change, the qualitative trend remains the same for different basis sets and methods (see Table 7). Adding an excess electron changes the bonding interaction from the O-end configuration to the H-end configuration, which significantly enhances the relative Raman intensity of the υ_4 mode with respect to the υ_5 mode.

One may use the Raman intensity of an isolated water molecule as a reference. With respect to the reference, the enhancement factors for the υ_4 mode are around 3000, 2300, and 130 in $H_2O\cdots M^-$ for M = Cu, Ag, and Au, respectively. These values are obviously larger than the corresponding enhancement factors of 40, 21, and 4 for the υ_5 mode of the anionic complexes. The results may be compared to the enhancement effects observed in the SERS spectra when waters adsorb on the Cu, Ag, and Au electrodes at negative potentals.[25−27] Our calculations demonstrate that the Raman intensity in an off-resonance Raman scattering process is very sensitive to the chemical effect, which, in turn, depends strongly on the adsorption configuration and the property of metal substrates.

Table 8 presents the isotropic and anisotropic polarizability derivatives of the H−O−H bending mode (υ_4) and the O−H stretching modes (υ_5 and υ_6) for the $H_2O\cdots M^-$ complexes calculated at the B3LYP/AVTZ/Lanl2DZ level. For the υ_6 mode, it is clear from Table 8 that it is the extraordinarily small anisotropic polarizability derivative for $H_2O\cdots Au^-$ that makes its Raman intensity the smallest among the three $H_2O\cdots M^-$ complexes. For the υ_5 mode, on the other hand, the anisotropic parts of all three are similar, but the magnitude of the isotropic polarizability derivative increases steadily in the order of Cu^-, Ag^-, and Au^-, leading to the sequence of $I_R(Cu^-) > I_R(Ag^-) > I_R(Au^-)$. For the υ_4 mode, we see that both the isotropic and the anisotropic polarizability derivatives increase in the same order of $Au^- < Ag^- < Cu^-$, such that $I_R(Cu^-) > I_R(Ag^-) > I_R(Au^-)$.

Conclusions

We have investigated the influence of the hydrogen bonding interactions on the vibrational Raman spectra of water in three kinds of anionic complexes. The hydrogen bonding interactions can induce significantly the vibrational frequency shifts and the Raman intensity changes when the water molecules are directly bound to the anions or an electron. Our results showed that the HB O−H stretching frequencies exhibit a significant red shift. This result can be interpreted well from the charge transfer to the antibonding orbital of the O−H bond. The extent of the red shift in the vibrational frequency is closely associated with the amount of charge transferred. Such a correlation is, however, not valid for the Raman intensity.

An interesting issue addressed in the present calculations is how to understand the influence of the hydrogen bond interaction on the Raman intensities of water. Although water acts as a proton donor as in $HOH\cdots X^-$ or $HOH\cdots M^-$, the polarizability of the proton acceptor, X^- or M^-, plays an important role. For the water···halide anionic complexes, their Raman intensities of the HB O−H stretching vibrations increase with the polarizabilities of halide anions. The strongest Raman signal should appear in $H_2O\cdots I^-$, in good agreement with the experimental observations. This is due to the hydrogen bonding interaction between H_2O and I^-, resulting in the largest isotropic polarizability derivatives along the O−H stretching mode. Along this series of F^-, Cl^-, Br^-, and I^-, the strongest Raman signal also appears in $H_2O\cdots I^-$ for the H−O−H bending vibration, because of the largest anisotropic polarizability derivatives. By analyzing the polarizability derivatives, we further suggest that the vibrational coupling between the H−O−H and $OH\cdots I^-$ bending modes contribute to enhancement of the Raman intensity of the H−O−H bending mode.

Another interesting issue investigated in the present work is the relative enhancement of the Raman intensity for the intramolecular bending mode of water with respect to that of the O−H stretching mode. For the systems studied here, the ratio of the Raman intensities between the H−O−H bending mode and the HB O−H stretching mode increases from 0.01 in the free water molecule to about 1 in the $H_2O\cdots Cu^-$ complex. This result demonstrates that for a proton-donor water molecule the enhancement effect in the Raman intensity is more significant for the bending mode than for its O−H stretching mode in the off-resonance Raman scattering processes. We believe that this observation is of general significance in other systems involving water molecules through the hydrogen bonding to a proton acceptor with large polarizability. A strong Raman signal of the H−O−H bending mode may be considered as a fingerprint to address the local microstructures of water molecules in the chemical and biological systems.

Acknowledgment. The authors gratefully thank the financial supports from NSF of China (No. 10474082, 20433040, and 20573087) and Ministry of Science and Technology (973 Program No.2007CB815303). D.Y.W. thanks the HPC of XMU. S.H.L. thanks the support from Academic Sinica and National Center for High-Performance Computing.

References and Notes

(1) (a) Blandame, M. J.; Fox, M. F. *Chem. Rev.* **1970**, *70*, 59. (b) Gopalakrishnan, S.; Liu, D.; Allen, H. C.; Kuo, M. J. *Chem. Rev.* **2006**, *106*, 1155.

(2) Cappa, C. D.; Smith, J. D.; Wilson, K. R.; Messer, B. M.; Gilles, M. K.; Cohen, R. C.; Saykally, R. J. *J. Phys. Chem. B* **2005**, *109*, 7046. Walrafen, G. E. In *Water: A comprehensive treatise*; Franks, F., Ed.; Plenum Press: New York, 1972; Vol. 1, pp 151−214. Chatzidimitriou-Dreismann, C. A.; Krieger, U. K.; Moller, A.; Stern, M. *Phys. Rev. Lett.* **1995**, *75*, 3008.

(3) Moskovits, M.; Michaelian, K. H. *J. Chem. Phys.* **1978**, *69*, 2306.

(4) Bartlett, J. S.; Voss, K. J.; Sathyendranath, S.; Vodacek, A. *Appl. Opt.* **1998**, *37*, 3324.

(5) (a) Faris, G. W.; Copel, R. A. *Appl. Opt.* **1997**, *36*, 2686. (b) Carey, D. M.; Korenowski, G. M. *J. Chem. Phys.* **1998**, *108*, 2669.

(6) (a) Busing, W. R.; Hornig, D. F. *J. Phys. Chem.* **1961**, *65*, 284. (b) Schultz, J. W.; Hornig, D. F. *J. Phys. Chem.* **1961**, *65*, 2131.

(7) Walrafen, G. E.; *J. Chem. Phys.* **1962**, *36*, 1035.

(8) Rull, F.; de Saja, J. A. *J. Raman Spectrosc.* **1985**, *17*, **167**.

(9) Weston, Jr. R. E. *Spectrochim. Acta* **1962**, *18*, 1257.

(10) Wall, T. T.; Hornig, D. F. *J. Chem. Phys.* **1966**, *45*, 3424.

(11) Liu, D.; Ma, G.; Levering, L. M.; Allen, H. C. *J. Phys. Chem. B* **2004**, *108*, 2252.

(12) Burikov, S. A.; Dolenko, T. A.; Velikotnyi, P. A.; Sugonyaev, A. V.; Fadeev, V. V. *Opt. Spectrosc.* **2005**, *98*, 235.

(13) Telle, H. R.; Laubereau, A. *Opt. Commun.* **1980**, *34*, 287.

(14) Yui, H.; Sawada, T. *Phys. Rev. Lett.* **2000**, *85*, 3512.

(15) Tauber, M. J.; Mathies, R. A. *J. Phys. Chem. A* **2001**, *105*, 10952.

(16) Mizuno, M.; Tahara, T. *J. Phys. Chem. A* **2001**, *105*, 8823.

(17) Tauber, M. J.; Mathies, R. A. *Chem. Phys. Lett.* **2002**, *354*, 518.

(18) Mizuno, M.; Tahara, T. *J. Phys. Chem. A* **2003**, *107*, 2411.
(19) Tauber, M. J.; Mathies, R. A. *J. Am. Chem. Soc.* **2003**, *125*, 1394.
(20) Mizuno, M.; Yamaguchi, S.; Tahara, T. *J. Phys. Chem. A* **2005**, *109*, 5257.
(21) Fleischmann, M.; Hendra, P. J.; Hill, I. R.; Pemble, M. E. *J. Electroanal. Chem.* **1981**, *117*, 243.
(22) Chen, T. T.; Smith, K. E.; Owen, J. F.; Chang, R. K. *Chem. Phys. Lett.* **1984**, *108*, 32.
(23) Kung, H. P.; Chen, T. T. *Chem. Phys. Lett.* **1986**, *130*, 311.
(24) Funtikov, A. M.; Sigalaev, S. K.; Kazarinov, V. E. *J. Electroanal. Chem.* **1987**, *228*, 197.
(25) Chen, Y. X.; Zou, S. Z.; Huang, K. Q.; Tian, Z. Q. *J. Raman Spectrosc.* **1998**, *29*, 749.
(26) Chen, Y. X.; Tian, Z. Q. *Chem. Phys. Lett.* **1997**, *281*, 379.
(27) Chen, Y. X.; Otto, A. *J. Raman Spectrosc.* **2005**, *36*, 736.
(28) Ayotte, P.; Weddle, G. H.; Kim, J.; Johnson, M. A. *J. Am. Chem. Soc.* **1998**, *120*, 12361.
(29) Choi, J. −H.; Kuwata, K. T.; Cao, Y. B.; Okumura, M. *J. Phys. Chem. A* **1998**, *102*, 503.
(30) (a) Robertson, W. H.; Johnson, M. A. *Ann. Rev. Phys. Chem.* **2003**, *54*, 173 and the references therein. (b) Hiraoka, K,; Mizuse, S.; Yamabe, S. *J. Phys. Chem.* **1988**, *92*, 3943.
(31) Xantheas, S. S. *J. Phys. Chem.* **1996**, *100*, 9703.
(32) (a) Ayotte, P.; Bailey, C. G.; Weddle, G. H.; Johnson, M. A. *J. Phys. Chem. A* **1998**, *102*, 3067. (b) Ayotte, P.; Weddle, G. H.; Bailey, C. G.; Johnson, M. A.; Vila, F.; Jordan, K. D. *J. Chem. Phys.* **1999**, *110*, 6268.
(33) Thompson, W. H.; Hynes, J. T. *J. Am. Chem. Soc.* **2000**, *122*, 6278.
(34) Ibach, H.; Lehwald, S. *Surf. Sci.* **1980**, *91*, 187.
(35) Avila, G. *J. Chem. Phys.* **2005**, *122*, 144310.
(36) Kim, J. S.; Suh, B.; Kim, K. S. *J. Chem. Phys.* **1999**, *111*, 10077.
(37) Herbert, J. M.; Head-Gordon, M. *J. Am. Chem. Soc.* **2006**, *128*, 13932.
(38) Adamo, C.; Lelj, F. *J. Mol. Struct. (Theochem)* **1997**, *389*, 83.
(39) Antusek, A.; Urban, M.; Sadlej, A. J. *J. Chem. Phys.* **2003**, *119*, 7247.
(40) Muntean, F.; Taylor, M. S.; McCoy, A. B.; Lineberger, W. C. *J. Chem. Phys.* **2004**, *121*, 5676.
(41) Taylor, M. S.; Muntean, F.; Lineberger, W. C.; McCoy, A. B. *J. Chem. Phys.* **2004**, *121*, 5688.
(42) Rathbone, G. J.; Sanford, T.; Andrews, D.; Lineberger, W. C. *Chem. Phys. Lett.* **2005**, *401*, 570.
(43) Schneider, H.; Boese, A. D.; Weber, J. M.; *J. Chem. Phys.* **2005**, *123*, 084307.
(44) Ranea, V. A.; Michaelides, A.; Ramirez, R.; Verges, J. A.; de Andres, P. L.; King, D. A. *Phys. Rev. B* **2004**, *69*, 205411.
(45) (a) Cabarcos, O. M.; Weinheimer, C. J.; Lisy, J. M.; Xantheas, S. S. *J. Chem. Phys.* **1999**, *110*, 5. (b) Chaban, G. M.; Xantheas, S. S.; Gerber, R. B. *J. Phys. Chem. A* **2003**, *109*, 4952.
(46) Amos, R. D. *Chem. Phys. Lett.* **1986**, *124*, 376.
(47) Knochenmuss, R.; Leutwyler, *J. Chem. Phys.* **1992**, *96*, 5233.
(48) Kim, K. S.; Mhin, B. J.; Choi, U.; Lee, K. *J. Chem. Phys.* **1992**, *97*, 6649.
(49) Hermansson, K. *J. Chem. Phys.* **1993**, *99*, 861.
(50) (a) Torii, H. *Phys. Rev. Lett.* **2000**, *84*, 5236. (b) Chatzidimitriou-Dreismann, C. A.; Abdul-Redah, T.; Kolaric, B. *Phys. Rev. Lett.* **2000**, *84*, 5237.
(51) Neumann, S.; Eisfeld, W.; Sobolewski, A.; Domcke, W. *Phys. Chem. Chem. Phys.* **2004**, *6*, 5297.
(52) (a) Becke, A. D. *J. Chem. Phys.* **1993**, *98*, 5648. (b) Lee, C.; Yang, W.; Parr, R. G. *Phys. Rev. B* **1988**, *37*, 785.
(53) Frisch, M. J.; Trucks, G. W.; Schlegel, H. B.; Scuseria, G. E.; Robb, M. A.; Cheeseman, J. R.; Montgomery, J. A., Jr.; Vreven, T.; Kudin, K. N.; Burant, J. C.; Millam, J. M.; Iyengar, S. S.; Tomasi, J.; Barone, V.; Mennucci, B.; Cossi, M.; Scalmani, G.; Rega, N.; Petersson, G. A.; Nakatsuji, H.; Hada, M.; Ehara, M.; Toyota, K.; Fukuda, R.; Hasegawa, J.; Ishida, M.; Nakajima, T.; Honda, Y.; Kitao, O.; Nakai, H.; Klene, M.; Li, X.; Knox, J. E.; Hratchian, H. P.; Cross, J. B.; Adamo, C.; Jaramillo, J.; Gomperts, R.; Stratmann, R. E.; Yazyev, O.; Austin, A. J.; Cammi, R.; Pomelli, C.; Ochterski, J. W.; Ayala, P. Y.; Morokuma, K.; Voth, G. A.; Salvador, P.; Dannenberg, J. J.; Zakrzewski, V. G.; Dapprich, S.; Daniels, A. D.; Strain, M. C.; Farkas, O.; Malick, D. K.; Rabuck, A. D.; Raghavachari, K.; Foresman, J. B.; Ortiz, J. V.; Cui, Q.; Baboul, A. G.; Clifford, S.; Cioslowski, J.; Stefanov, B. B.; Liu, G.; Liashenko, A.; Piskorz, P.; Komaromi, I.; Martin, R. L.; Fox, D. J.; Keith, T.; Al-Laham, M. A.; Peng, C. Y.; Nanayakkara, A.; Challacombe, M.; Gill, P. M. W.; Johnson, B.; Chen, W.; Wong, M. W.; Gonzalez, C.; Pople, J. A. *Gaussian 03*, revision C.02; Gaussian, Inc.: Wallingford, CT, 2004.
(54) (a) Hay, P. J.; Wadt, W. R. *J. Chem. Phys.* **1985**, *82*, 270. (b) Wadt, W. R.; Hay, P. J. *J. Chem. Phys.* **1985**, *82*, 284. (c) Hay, P. J.; Wadt, W. R. *J. Chem. Phys.* **1985**, *82*, 299.
(55) Woon, D. E.; Dunning, T. H., Jr. *J. Chem. Phys.* **1993**, *98*, 1358.
(56) (a) Stevens, W.; Basch, H.; Krauss, J. *J. Chem. Phys.* **1984**, *81*, 6026. (b) Stevens, W. J.; Krauss, M.; Basch, H.; Jasien, P. G. *Can. J. Chem.* **1992**, *70*, 612. (c) Cundari, T. R.; Stevens, W. J. *J. Chem. Phys.* **1993**, *98*, 5555.
(57) Boys, S. F.; Bernardi, F. *Mol. Phys.* **1970**, *19*, 553.
(58) Simon, S.; Duran, M.; Dannenberg, J. J. *J. Chem. Phys.* **1996**, *105*, 11024.
(59) Reed, A. E.; Curtiss, L. A.; Weinhold, F. *Chem. Rev.* **1988**, *88*, 899.
(60) Pulay, P.; Fogarasi, G.; Pang, F.; Boggs, J. E. *J. Am. Chem. Soc.* **1979**, *101*, 2550.
(61) (a) Van Straten, A. J.; Smit, W. M. *J. Mol. Spectrosc.* **1975**, *56*, 484. (b) Bogaard, M. P.; Haines, R. *Mol. Phys.* **1980**, *41*, 1281.
(62) Backskay, G. B.; Saebo, S.; Taylor, P. R. *Chem. Phys.* **1984**, *90*, 215.
(63) (a) Hu, J. H.; Wang, G. Z. *Computational Principles and Programs of Infrared and Raman Spectroscopy*; Editorial Office of Spectroscopy and Spectral Analysis. (b) Wilson, E. B., Jr.; Decius, J. C.; Cross, P. C. *Molecular Vibrations*; McGraw-Hill: New York, 1955.
(64) Zilles, B. A.; Person, W. B. *J. Chem. Phys.* **1983**, *79*, 65 and references therein.
(65) Schrotter, H. W.; Klockner, In *Raman Spectroscopy of Gases and Liquids*; Weber, A., Ed.; Springer-Verlag: Berlin, 1979; pp 123−166.
(66) (a) Hoy, A. R.; Bunker, P. R. *J. Mol. Spectrosc.* **1974**, *52*, 439. (b) Hoy, A. R.; Bunker, P. R. *J. Mol. Spectrosc.* **1975**, *59*, 159 (erratum).
(67) (a) Tennyson, J.; Zobov, N. F.; Williamson, R.; Polyansky, O. L.; Bernath, P. F.; *J. Phys. Chem. Ref. Data.* **2001**, *30*, 735. (b) Buchitsu, K.; Morino, Y. *Bull. Chem. Soc. Jpn.* **1965**, *38*, 1521. (c) Shirin, S. V.; Polyansky, O. L.; Zobov, N. F.; Ovsyannikov, R. I.; Csaszar, A. G.; Tennyson, J. *J. Mol. Spectrosc.* **2006**, *236*, 216.
(68) (a) Murphy, W. F. *Mol. Phys.* **1977**, *33*, 1701. (b) Murphy, W. F. *Mol. Phys.* **1978**, *36*, 727.
(69) Zilles, B. A.; Person, W. B. *J. Chem. Phys.* **1983**, *79*, 65 and references therein.
(70) (a) Alia, J. M.; Edwards, H. G. M. *Int. J. Quantum Chem.* **2007**, *107*, 1170. (b) Alia, J. M.; Edwards, H. G. M. *J. Phys. Chem. A* **2005**, *109*, 7977. (c) Wu, D. Y.; Hayashi, M.; Lin, S. H.; Tian, Z. Q. *Spectrochim. Acta A* **2004**, *60*, 137.
(71) Kim, J.; Lee, J. Y.; Oh, K. S.; Park, J. M.; Lee, S.; Kim, K. S. *Phys. Rev. B* **1999**, *59*, R930.
(72) Xantheas, S. *J. Chem. Phys.* **1999**, *102*, 4505.
(73) Xu, X.; Goddard, W. A., III. *J. Phys. Chem. A* **2004**, *108*, 2305.
(74) Schofield, D. P.; Lane, J. R.; Kjaergaard, H. G. *J. Phys. Chem. A* **2007**, *111*, 567.
(75) Wuelfert, S.; Herren, D.; Leutwyler, S. *J. Chem. Phys.* **1987**, *86*, 3751.
(76) Hirabayashi, S.; Yamada, K. M. T. *J. Chem. Phys.* **2005**, *122*, 244501.
(77) (a) Roscioli, J. R.; Johnson, M. A. *J. Chem. Phys.* **2007**, *126*, 024307. (b) Roscioli, J. R.; Hammer, N. I.; Johnson, M. A. *J. Phys. Chem. A* **2006**, *110*, 7517.
(78) Roscioli, J. R.; Diken, E. G.; Johnson, M. A.; Horvath, S.; McCoy, A. B. *J. Phys. Chem. A* **2006**, *110*, 4944.
(79) Craig, J. D. C. *J. Raman Spectrosc.* **2002**, *33*, 191.
(80) Frediani, L.; Mennucci, B.; Cammi, R. *J. Phys. Chem. A* **2004**, *108*, 13796.
(81) Valderrama, E.; Wheatley, R. J. *J. Comput. Chem.* **2003**, *24*, 2075.
(82) Frederikse, H. P. R.; *CRC Handbook of Chemistry and Physics*; Lide, D. R.; CRC Press: Boca Raton, FL, 2003; pp 12−17.
(83) Papai, I. *J. Chem. Phys.* **1995**, *103*, 1860.
(84) Kauffman, J. W.; Hauge, R. H.; Margrave, J. L. *J. Phys. Chem.* **1985**, *89*, 3541.
(85) Neogrady, P.; Urban, M.; Sadlej, A. J. *J. Mol. Struct.(Theochem*) **1995**, *332*, 197.
(86) Yang, M.; Jackson, K. A. *J. Chem. Phys.* **2005**, *122*, 184317.
(87) Schwerdtfeger, P.; Bowmaker, G. A. *J. Chem. Phys.* **1993**, *100*, 4487.
(88) Kello, V.; Urban, M.; Sadlej, A. J. *Chem. Phys. Lett.* **1996**, *253*, 383.
(89) Neogrady, P.; Kello, P.; Urban, M.; Sadlej, A. J. *Int. J. Quantum Chem.* **1997**, *63*, 557.